Microstructure, Mechanical Properties of Extruded Aluminum at Different Ram Speeds in Micro/Meso-Scale

Walaa Abdel-Aziem[1], Mohsen A. Hassan[2], Takehiko Makino[3] , Atef Hamada[4]

Abstract
Commercially pure aluminum was deformed via the extrusion process at different strain rates considering the temperature rising during the deformation, i.e., with different Zener–Hollomon parameters (*Z*), to investigate the effect of *Z* on its grain structure and tensile properties in the micro/meso-scale. The results demonstrate that deformation-induced grain refinement was obtained by increasing the values of the *Z*. Besides, the dislocation density of the aluminum specimens increased with the strain rate which is in conformity with the Orowan equation. An apparent increment in yield and tensile strength was observed in the deformed aluminum with increasing the value of *Z* parameter. This can be attributed to two strengthening mechanisms, i.e., by combining the Hall–Petch relation (strain hardening due to the grain refining) and Taylor equation (owing to dislocation–dislocation interactions).

Keywords Micro/meso-extrusion · Plastic deformation · Zener · Hollomon parameter · Dislocation density · Mechanical properties · Aluminum

Introduction

Recently, miniaturization has played a significant role in revolutionizing numerous fields of technology by advancing novel applications in electronics, biotechnology, healthcare, etc. The going trend toward miniaturization makes the demand for microparts growing at an unprecedented rate.

As reported by technical analysts, the annual turnover for the microparts industry alone is estimated to bring 27 billion dollars milestones by 2022 [1]. Among the production techniques for microparts, micro-extrusion has the advantages of high production rate, repeatability, and effective material utilization. In spite of its potential, the basic manufacturing characteristics of the microforming process is still limited because of the difficulties to scale down all parameters referring to the theory of similarity because of the size effects [2–10].

Even though macro-extrusion is well established and has been comprehensively studied. However, these concepts cannot be directly applied to the micro/meso-scale. Thus, wide-ranging testing and study of the material behavior in the micro/meso-scale are extensively needed to attain fundamental knowledge as the length-scales converge. Both the microstructure and the stress properties which affect the material behavior are significantly related to the extrusion conditions such as extrusion speed. S. Rahim also studied the extrusion speed and temperature through the hot extrusion of AA 6061 alloy [11].

Gagliardi et al. reported that the ram velocity affects the grain sizes and tensile properties of AA6060 alu- minum alloy [12]. Zhao et al. studied the effect of defor- mation speed on the microstructure and mechanical properties during continuous extrusion for AA6063 and demonstrated that there is an optimum extrusion wheel velocity to process the components with good mechanical properties [13]. Junquan Yu et al. found that increasing

✉ Walaa Abdel-Aziem
walaa.abdelaziem@gmail.com

[1] Department of Mechanical Design and Production Engineering, Faculty of Engineering, Zagazig University, P.O. Box 44519, Zagazig, Egypt

[2] Egypt-Japan University of Science and Technology, P. O. Box 179, New Borg El-Arab City 21934, Alexandria, Egypt

[3] Department of Mechanical Engineering, Nagoya Institute of Technology, Gokiso-cho, Showa-ku, Nagoya, Aichi 466-8555, Japan

[4] Kerttu Saalasti Institute, University of Oulu, Pajatie 5, 85500 Nivala, Finland

billet heating temperature and extrusion speed by conducting the Porthole die extrusion process triggered the formation of new grains within the bonding interface as well as enhanced the hardness, strength and ductility of the extruded profiles [14]. C.Hinesley et al. investi- gated the influence of temperature and ram speed on the flow pattern during conducting axisymmetric extrusions of 2024 Al alloy [15]. WU Xiang et al. investigated the influence of extrusion speed on Aluminum profile extrusion processes [16]. Trond Furu et al. also investigated the effect of the extrusion speed on the texture of AA6082 alloy [17]. Evidently, extrusion speed is one of the crucial parameters that can affect the deformation behavior dur- ing the extrusion process. However, the above-mentioned works have been conducted to study the deformation characteristics of Al alloys in macro-scale extrusion. Nevertheless, for micro/meso-extrusion, a systematic investigation of the microstructure and mechanical properties in terms of extrusion speeds has not yet been thoroughly studied.

To realize this goal, this study provides an in-depth understanding of the effect of the extrusion speed on the microstructure characteristics and tensile properties of aluminum 1070 alloy at different extrusion speed in the micro/meso-scale. Additionally, Zener–Hollomon parameter was used to investigate the effect of strain rate on both the grain structure and the tensile properties of the deformed Al specimens. Besides, the dislocation density was investigated for the processed specimens at different speeds.

Experimental Study

In this study, aluminum 1070 alloy was received as hot-rolled rods of 1.5 ϕ mm × 300 mm. The as-received specimens were heat-treated at 350 °C and then cooled to room temperature to get rid of any previous work-hardening effects. The length of the starting materials for micro/meso-scale extrusion (MMSE) is 6 mm. The specimens were extruded from 1.5 to 1 mm using a micro-extrusion die at four different speeds of 1, 5, 10, and 15 mm/min at room temperature.

The micro-extrusion die used in this study consists of two halves of die blocks with a circular cross section. The micro/meso-extrusion die had a distinct design in which the two halves of the die were cut horizontally and not as in conventional extrusion dies where the two halves are cut vertically.

The two halves of die blocks were assembled in the container and then by means of base plate attached together by screws, thus avoiding assembling and disassembling of parts in each extrusion process. One auxiliary sample of 6 mm in length was used to assist the deformed sample in getting out of the extrusion die, as shown in Fig. 1a. This design has the advantage of eliminate the burrs that can easily be formed if the die was cut vertically into two halves, and as a result reducing the pressing force as well as accomplishing high precision of the specimen shape after the extrusion process.

Hsu et al. [18] reported that the geometry of the die and the punch can affect the shape and precision of the produced specimens. The appearance of the actual experimental equipment can be shown in Fig. 1b and c. The

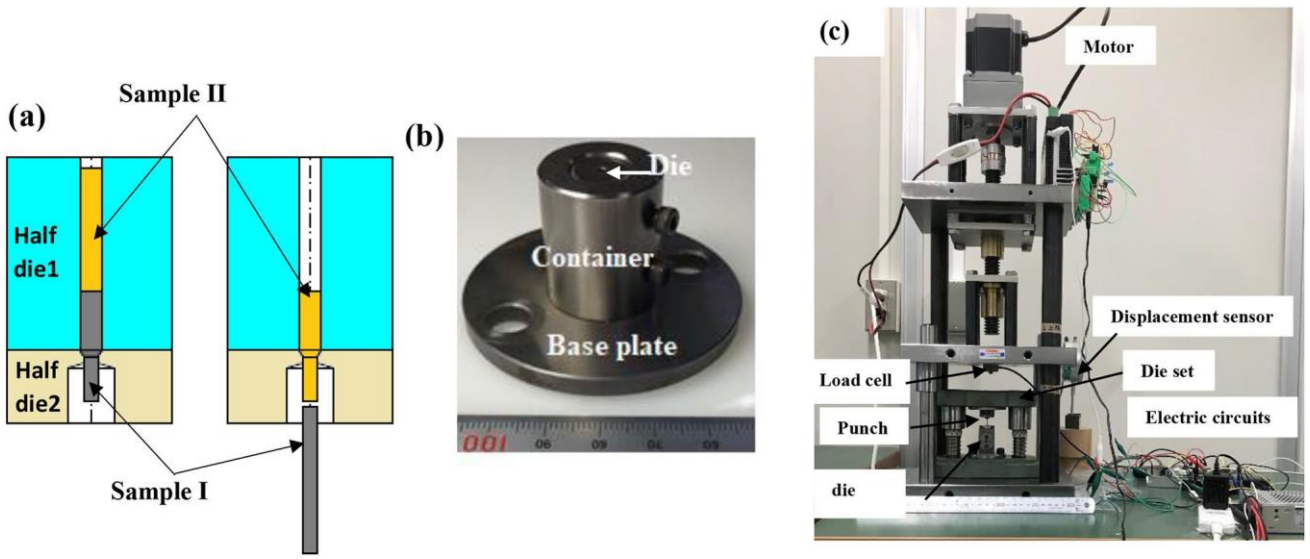

Fig. 1 (**a**) Schematic illustration of the extrusion die used in this study, (**b**) The typical implemented die and (**c**) the employed experimental setup.

specimens are lubricated with high kinematic viscosity oil, i.e., 430 mm^2/s at 313 K to minimize the frictional effect.

The grain structure of the processed Aluminum 1070 after the MMSE process was characterized by electron backscatter diffraction (EBSD) detector attached on a JEOL JSM-7001F field emission scanning electron micro- scope (SEM), with an operating voltage of 15 kV, a step size of 0.3 μm and a scanning area of 150 × 150 μm.

The specimens for all measurements were cut from the rods parallel to the extrusion direction. The EBSD measurements such as microstructure and texture evolution were characterized by TSL-OIM Data Analysis software.

For EBSD analysis, the surface of each specimen was ground on SiC abrasive paper and then mechanically polished with 0.04 μm colloidal alumina. X-ray diffraction analysis of the extruded aluminum rods was implemented on a Philips X pert Pro diffractometer using Cu-Kα radiation (λ = 0.15406 nm) at 45 kV and 200 mA settings. The crystallite size and dislocation density were measured by using the Williamson-Hall method [19, 20] according to the following equation, proceeding from the calculation of volume-weighted average domain size,D_v and the micro-strain, according to the following equation [21]:

$$f3\cos\theta = \frac{K}{D_V} + 2E\left(\frac{2\sin\theta}{}\right)^{J}, \quad (1)$$

where $/3$ is the full width at half maximum height (FWHM), θ is the Bragg's angle of the peak, and l is the wavelength of X-ray (0.15406 nm), and k is the shape factor (0.9). By

plotting the $f]\cos\theta$ versus 4 sin θ, the values of D_v and can be determined from the slope and the ordinate intersection, respectively. Based on the Rietveld method [22], the average dislocation density can be calculated using the relation

$p = (p_D\ p_s)^{2}$, where p_D is the dislocation density due to the domain, $p_D = 3/D_v^2$ and p_s is the dislocation density due to strain within the microstructure, $p_s = E^2/b^2$, and b is the Burger's vector.

Finally, mechanical properties were investigated by uniaxial tensile testing to study the effect of extrusion speed on the as-processed aluminum 1070 alloy. A special micro/meso-scale tensile machine was fabricated by the Makino group in Nagoya Institute of Technology (NITech, Japan). Because the specimens have very small diameters of 1 mm making them difficult to be machined, the dog-bone shape for the specimens was produced by the adhesive method in which the two aluminum tubes were inserted at both sides of aluminum rod (the specimen) glued by an adhesive (acrylic adhesive, AY-123) from Cemedine Co. company, Japan. Details of the tensile machine and preparing the samples can be found in our published works [23]. The gauge length and diameter of the tested speci- men are 2 mm and 1 mm as shown in Fig. 2. The test was conducted at ambient temperature and at a strain rate of $1.6 \times 10^{-3}\ s^{-1}$.

Results and Discussion

Microstructure of Al Alloys

The initial microstructure of the as-received aluminum 1070 is illustrated in our previous work [24] which displays coarse grains with a random orientation relationship. Fig- ure 3a depicts the IPF maps of specimens after extrusion process at different speeds. It is observed that the grain size of aluminum 1070 alloy depends on the extrusion speed. The average grain sizes are 28.77, 27.94, 25.47, and 22.67 μm corresponding to the extrusion speeds of 1, 5, 10, and 15 mm/min, respectively. Thus, the grain size is decreasing with the increase of extrusion speed.

To describe the effect of extrusion speeds on the grain structure of aluminum 1070, Zener–Hollomon (Z) parameter is considered to be significant and effective in relating the grain size (d, μm) with the strain rate ($\dot{\varepsilon}$) which is given by the following equations [25, 26]:

$$d = AZ^{-n} \quad (2)$$

$$Z = \dot{\varepsilon} = \exp\left(\frac{Q}{RT}\right), \quad (3)$$

where A is a constant, n is the power-law exponent, T is the deformation temperature, Q is the related activation energy (96.15 kJ mol^{-1} for aluminum [27]), R is the gas constant. $\dot{\varepsilon}$ is the strain rate which can be determined by

following the equation proposed by Feltham [28]:

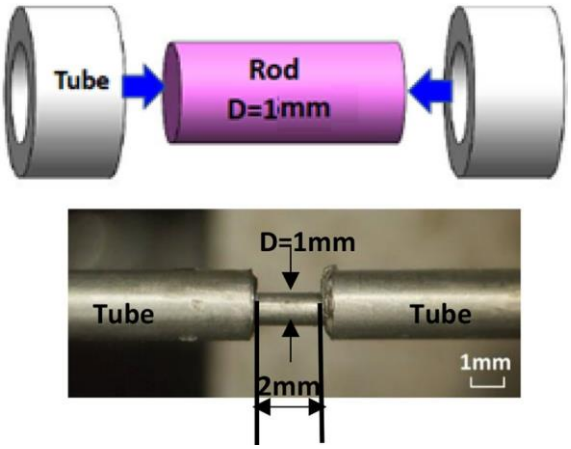

Fig. 2 Preparation of bone-shape sample and a typical appearance of the sample tensile test.

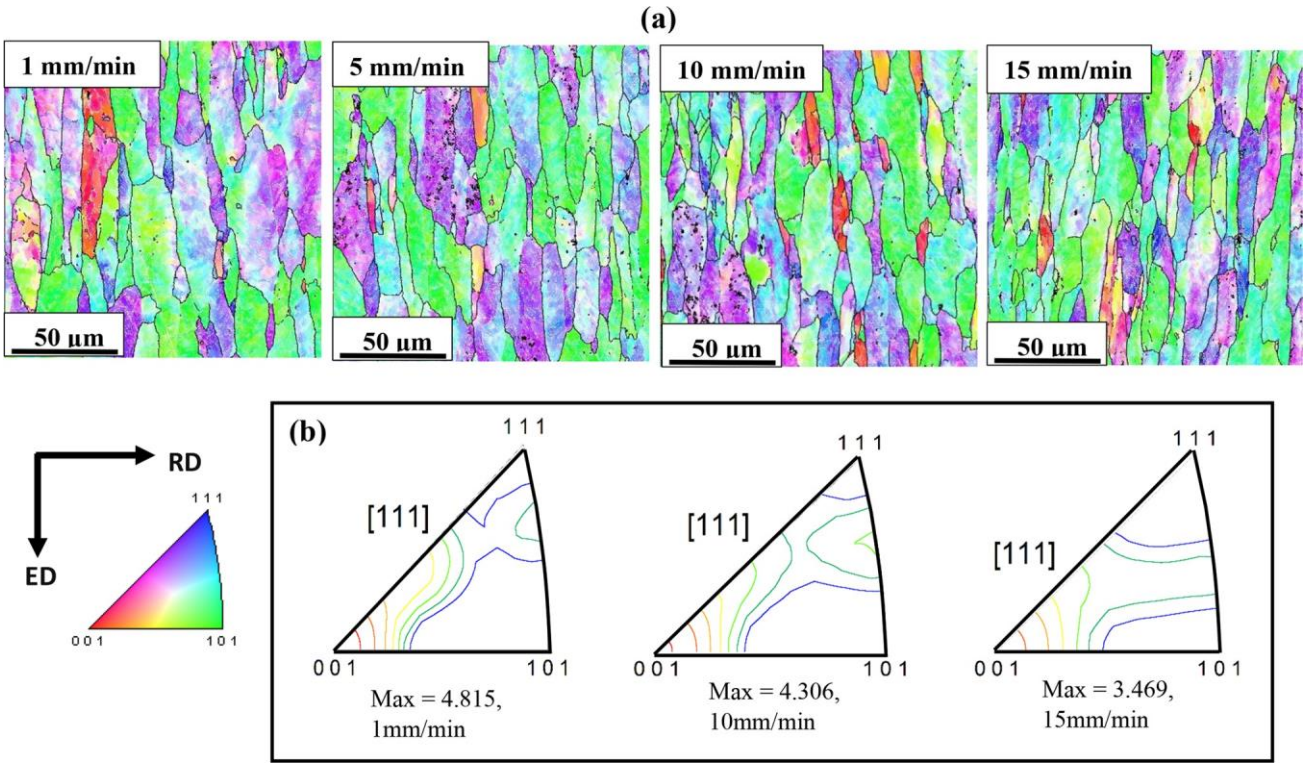

Fig. 3 (**a**) IPF maps of aluminum 1070 extruded at different speeds, and (**b**) the corresponding inverse pole figures of the extruded alloy. ED is the extrusion direction and RD radial direction.

$$\dot{\bar{\varepsilon}} = \frac{6D_B^2 V_R \ln ER}{D_B^3 - D_E^3}, \quad (4)$$

where V_R is the extrusion speed, ER is the extrusion ratio, and D_B and D_E are the diameters of the billet and extrudate, respectively. Here, the actual temperature (T_a) was utilized rather than the nominal deformation temperature (T) that can be determined by the following:

$$T_a = T + \Delta T, \quad (5)$$

where ΔT is the strain-induced temperature rise which the deformation is regarded as adiabatic, i.e., no heat transfer to the surrounding. Although the temperature rise during deformation is small, we considered it in our calculations for more accurate estimations. The temperature rise during deformation is given by [29]:

$$\Delta T = \frac{\alpha \int \bar{\sigma} d\bar{\varepsilon}}{\rho C} = \frac{\alpha \bar{\sigma}_a \bar{\varepsilon}}{\rho C}, \quad (6)$$

where α is the fraction of energy stored as heat, ρ is the density of the specimen, C is the mass heat capacity and $\bar{\sigma}_a$ is defined as the average value of $\bar{\sigma}$ over the strain interval 0 to $\bar{\varepsilon}$.

The strain rate and the values of ln Z under the extrusion conditions implemented in this study are listed in Table 1. As provided in Table 1, the calculated values of ln Z are 36.124, 37.64, 38.27, and 38.63 for the extrusion speeds of 1, 5, 10, and 15 mm/min, respectively. It is obvious here that ln Z becomes higher as the extrusion speeds increase,

Table 1 Extrusion and tensile properties of the aluminum 1070 alloy extruded at different speeds.

Extrusion speed, mm/min	Extrusion properties			Grain size	Tensile properties		
	ΔT, K	$\dot{\bar{\varepsilon}}$, s^{-1}	ln Z	d, μm	YS, MPa	UTS, MPa	El, %
1	6.535	0.077	36.124	28.77	155.6	185.3	21
5	6.7	0.384	37.64	27.94	166.5	197.2	19.5
10	7.144	0.768	38.27	25.47	173.3	209.5	18.5
15	7.509	1.15	38.63	22.67	180	217.8	17

in another word, as the strain rate increases. As stated in Eq. 2, that the average grain size (d) is a function of ln Z, which can be reformulated in the form: $\ln d = A - n \cdot \ln Z$.

From the information listed in Table 1, it can be said that the Z parameter affects the microstructure of the deformed aluminum 1070 alloy as the structure becomes relatively finer with higher values of ln Z that can be realized from the mechanism of grain refinement induced by plastic strain during the micro/meso-extrusion. In the deformation processing of aluminum 1070 at low strain rate (quasi-static) and at room temperature or above, i.e., low values of Z parameter, the refinement of grain structure is dominated by dislocations activities in the interior of grains which including forming of dislocation cells, dense walls, cell-blocks, geometry necessary boundaries (GNB, boundaries formed by statistical trapping of dislocations) and incidental dislocation boundaries (IDB, boundary between the neighboring cell-blocks) [30–32]. These dislocation cells gradually turn into subgrains with low angle grain boundaries (LAGBs, $2° \leq \theta \leq 15°$), within the interior of grains [24, 32–34] divided by boundaries of small misorientations. With increasing the strain, the subgrains rotate into high angle grain boundaries (HAGBs) with misorientation angle of $\theta \geq 15°$ and subsequently, new finer grains are generated within the parent grains. This can be clarified by the decrease in the texture intensity with increasing the strain rate, see Fig. 3b.

For that sense, it is interesting here to assess the dislocation density and the misorientation of all boundaries in the structure obtained from the EBSD analysis at different strain rates, as can see in Fig. 4. It is seen that the fraction of HAGBs is triggered by increasing the strain rate. Additionally, with increasing the strain rate, i.e., higher Z parameters, the dislocation density increases from about 1.95×10^{14} m^{-2} (strain rate, 0.077 s^{-1}) to 2.55×10^{14} m^{-2} (strain rate, 1.15 s^{-1}). The dislocation density (p) and the strain rate are related by the Orowan equation as follows [35, 36].

$$\varepsilon \approx b\rho s, \tag{7}$$

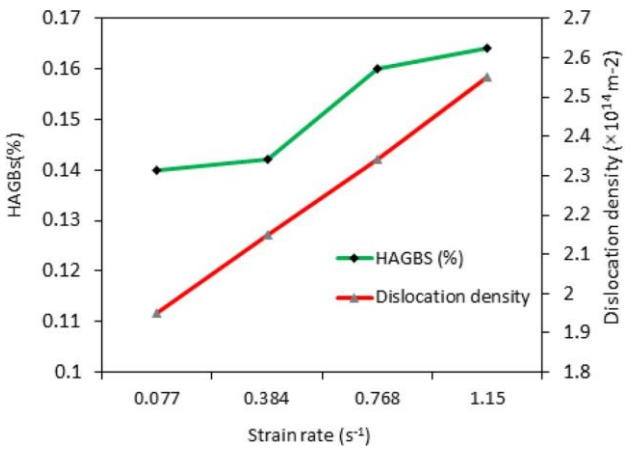

Fig. 4 HAGBs and the dislocation density for Al specimens deformed with different strain rates.

where s is the dislocation velocity, b is the burgers vector. The increase of dislocation density with increasing strain rate is in a line with the results presented in [36–38]. In this study, it is obvious that the degree of strain rate increment was higher than that of the dislocation density as shown in Table 1, that can be interpreted by the dislocation activ- ity in terms of activation volume that, in turns, depends on the temperature, time, and strain rate [39]. The activation volume for deformation of materials exhibiting bcc structures is in the range of (5–100 b^3), whereas the activation volume for fcc materials was about 10 to 100 times higher [40, 41]. Besides, the activation volume of the bcc materials is independent of the strain, whereas that for the fcc materials such as Al decreased as the strain increased [36, 41]. Moreover, the activation volume at different strain rates can be explained by the combined operation of the Peierls mechanism and dislocation drag mechanism. At strain rates less than 10^3 s^{-1}, the contribution of the dislocation drag process was small. Thus, the dislocation activity in this study was ascribed to the Peierls mechanism.

Mechanical Properties

The tensile stress–strain curves at room temperature of the aluminum 1070 alloys extruded at different speeds are presented in Fig. 5a. The yield strength (YS) and the ultimate tensile strength (UTS) increase with increasing the extrusion speed, but the elongation (El%) is slightly decreased. The extruded specimens show very small uniform elongation (about 1–2%, peak in the curves) which is similar behavior to the Al specimens deformed by other approaches [42–44]. This behavior is attributed to an insufficient ability of the materials to strain harden during deformation, resulting in commencing of early necking [38]. As summarized in Table 1, an increasing tensile strength corresponds to higher values of ln Z. This behavior can be mainly ascribed to the grain refinement accompanied by dislocation density which increases with an increase of ln Z. Higher strain rate achieved refining grain structure which, in turn, triggered numerous grain boundaries. These boundaries are acting as a barrier for slipping during the extrusion process and as a result the strength increases. Moreover, the dislocation density (p) increases with higher strain rates as in Fig. 4 that activates the interaction between dislocations, and as a result, the strength increases. The yield strength (σ_y) can be related to these two strengthening mechanisms by combining the Hall–Petch relation (strain hardening due to the grain

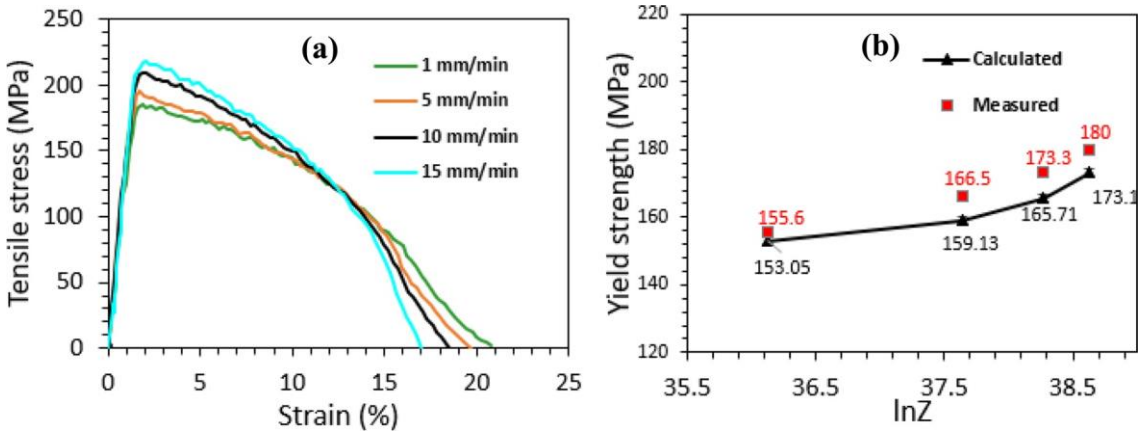

Fig. 5 (**a**) Engineering stress–strain curves of the speeds, and (**b**) The calculated and experimentally measured yield strength aluminum specimens as a function of ln *Z*.

refining) and Taylor equation (owing to dislocation–dislocation interactions) as follows [45, 46]:

$$\sigma_y = \sigma_0 + \alpha MGb\sqrt{\rho} + K_y d^{-1/2}, \quad (8)$$

where (σ_0 is the stress constant due to the lattice friction (20 MPa), α is a characteristic of dislocation–dislocation interaction strength (taken as 0.5), M is the Taylor factor (taken as 3.06 for Al [47]), G is the shear modulus (27 GPa), b is the burgers vector (0.286 nm for Al [45]),K_y is the Hall–Petch coefficient (0.04 MPa $m^{1/2}$) for Al [45]), and d the grain size.

The yield strength values of the extruded aluminum 1070 specimens with different Z values can then be calculated in terms of Eq. 8. The experimentally measured and calculated values of the yield strength are presented in Fig. 5b as a function of ln Z. The calculated yield strength is shown to agree reasonably with the measured values for the specimens with different ln Z. This is in a line with the result of Li et al. [38], where, the yield strength of the deformed Cu increases with increasing the value of ln Z. Thus, it is concluded that the deformed Al specimens with higher Z values are strengthened by the two mechanisms, i.e., the grain refinement and dislocation strengthening.

Conclusions

In this study, different strain rates were implemented via micro/meso-scale extrusion and the effect of the strain rate on the grain structure and tensile properties of aluminum 1070 alloy were studied. The following conclusions can be briefly summarized as follows:

1. The grain structure of the aluminum 1070 was refined with a higher fraction of high angle grain boundaries by increasing strain rate. The average grain sizes are 28.77, 27.94, 25.47, and 22.67 μm corresponding to the extrusion speeds of 0.077, 0.384, 0.768, and 1.15 mm/min, respectively.

2. The dislocation density of the aluminum 1070 alloy increased with the strain rate as quantified by the Orowan equation. The dislocation density increases from about 1.95×10^{14} m^{-2} (strain rate, 0.077 s^{-1}) to 2.55×10^{14} m^{-2} (strain rate, 1.15 s^{-1}).
3. With increasing the value of ln Z, the yield and ultimate strength of the extruded Al increase due to the grain refinement along with the dislocation–dislocation interactions.

Acknowledgement The authors would like to acknowledge the financial support from the Missions Sector-Higher Education Ministry, Egypt, through this work.

References

1. A. Dhal, S. Panigrahi, M. Shunmugam, Achieving excellent microformability in aluminum by engineering a unique ultrafine-grained microstructure. Sci. Rep. **9**, 10683 (2019)
2. Z. Jiang, J. Zhao, H. Lu, D. Wei, K.-I. Manabe, X. Zhao, X. Zhang, D. Wu, Influences of temperature and grain size on the material deformability in microforming process. Int. J. Mater. Form. **10**, 753–764 (2017)
3. J. Zhao, H. Xie, H. Lu, Z. Jiang, Size effects in micro rolling of metals (2017)
4. W.L. Chan, M. Fu, B. Yang, Study of size effect in micro-extrusion process of pure copper. Mater. Des. **32**, 3772–3782 (2011)
5. S.A. Parasiz, B. Kinsey, N. Krishnan, J. Cao, M. Li, Investigation of deformation size effects during microextrusion (2007)
6. N. Krishnan, J. Cao, K. Dohda, Study of the size effect on friction conditions in microextrusion—part I: microextrusion experiments and analysis (2007)

7. D. Rajenthirakumar, R. Sridhar, R. Abenethiri, R. Kartik, D. Bagri, Experimental investigations of grain size effects in forward microextrusion. Int. J. Adv. Manuf. Technol. **85**, 2257–2264 (2016)
8. Z. Yao, D. Mei, P. Tang, Z. Chen, On the size effects in micro/meso semisolid extrusion–forging of A356 aluminum alloy. Int. J Adv. Manuf. Technol. **73**, 1243–1252 (2014)
9. H. Lu, D. Wei, Z. Jiang, X. Liu, K. Manabe, Modelling of size effects in microforming process with consideration of grained heterogeneity. Comput. Mater. Sci. **77**, 44–52 (2013)
10. T. Yalçinkaya, İ Özdemir, I. Simonovski, Micromechanical modeling of intrinsic and specimen size effects in microforming. Int. J. Mater. Form. **11**, 729–741 (2018)
11. S. Rahim, M. Lajis, S. Ariffin, Effect of extrusion speed and temperature on hot extrusion process of 6061 aluminum alloy chip. ARPN J. Eng. Appl. Sci. **11**, 2272–2277 (2016)
12. F. Gagliardi, T. Citrea, G. Ambrogio, L. Filice, Influence of the process setup on the microstructure and mechanical properties evolution in porthole die extrusion. Mater. Des. **60**, 274–281 (2014)
13. Y. Zhao, B. Song, J. Pei, C. Jia, B. Li, G. Linlin, Effect of deformation speed on the microstructure and mechanical properties of AA6063 during continuous extrusion process. J. Mater. Process. Technol. **213**, 1855–1863 (2013)
14. J. Yu, G. Zhao, W. Cui, C. Zhang, L. Chen, Microstructural evolution and mechanical properties of welding seams in aluminum alloy profiles extruded by a porthole die under different billet heating temperatures and extrusion speeds. J. Mater. Process. Technol. **247**, 214–222 (2017)
15. C. Hinesley, H. Conrad, Effects of temperature and ram speed on the flow pattern in axisymmetric extrusions of 2024 Al alloy. Mater. Sci. Eng. **12**, 47–58 (1973)
16. W.X.-H.G.-Q. Sheng Lou, S.-M. Xin-Wu, The influence of extrusion speed and frictional status on Aluminum profile extrusion processes. *J. Plast. Eng*. 1 (2007).
17. T. Furu, Ø. Sødahl, E. Nes, L. Hanssen, O. Lohne, The influence of the extrusion speed on texture in the surface layer of aluminium profiles investigated by the EBSP technique, Materials Science Forum, Trans Tech Publ, 1994, pp. 1197–1204
18. M.-H. Hsu, K.-M. Huang, T.-C. Chen, J.-P. Wang, Manufacturing technology for the high-precision right-angle square body. Int. J. Adv. Manuf. Technol. **103**, 4055–4061 (2019)
19. G. Williamson, W. Hall, X-ray line broadening from filed aluminium and wolfram. Acta Metall. **1**, 22–31 (1953)
20. B. Tolaminejad, K. Dehghani, Microstructural characterization and mechanical properties of nanostructured AA1070 aluminum after equal channel angular extrusion. Mater. Des. **34**, 285–292 (2012)
21. P. Mukherjee, A. Sarkar, P. Barat, S. Bandyopadhyay, P. Sen, S. Chattopadhyay, P. Chatterjee, S. Chatterjee, M. Mitra, Deformation characteristics of rolled zirconium alloys: a study by X-ray diffraction line profile analysis. Acta Mater. **52**, 5687–5696 (2004)
22. P. Sahu, Lattice imperfections in intermetallic Ti-Al alloys: an X-ray diffraction study of the microstructure by the Rietveld method. Intermetallics. **14**, 180–188 (2006)
23. W. Abdel-Aziem, A. Hamada, T. Makino, M.A. Hassan, Micro/Meso-scale equal channel angular pressing of Al 1070 alloy: microstructure and mechanical properties. J. Mater. Eng. Perform. **29**, 6201–6211 (2020)
24. W. Abdel-Aziem, A. Hamada, T. Makino, M.A. Hassan, Microstructure evolution of AA1070 aluminum alloy processed by micro/meso-scale equal channel angular pressing. Met. Mater. Int. 1–13 (2019)
25. L. Tong, M. Zheng, L. Cheng, D. Zhang, S. Kamado, J. Meng, H. Zhang, Influence of deformation rate on microstructure, texture and mechanical properties of indirect-extruded Mg-Zn-Ca alloy. Mater. Charact. **104**, 66–72 (2015)
26. S.H. Park, B.S. You, R.K. Mishra, A.K. Sachdev, Effects of extrusion parameters on the microstructure and mechanical properties of Mg-Zn-(Mn)-Ce/Gd alloys. Mater. Sci. Eng. A. **598**, 396–406 (2014)
27. Y. An-Chou, C. Ho-Chieh, K. Chen-Ming, Static recovery activation energy of pure aluminum at room temperature. J. Eng. Mater. Technol. **136**, 034501 (2014)
28. P. Feltham, Extrusion of metals, metal treatment and drop. Forging. **23**, 440–444 (1956)
29. W.F. Hosford, R.M. Caddell, *Metal Forming: Mechanics and Metallurgy* (Cambridge University Press, Cambridge, 2011)
30. P. Hurley, F. Humphreys, The application of EBSD to the study of substructural development in a cold rolled single-phase aluminium alloy. Acta Mater. **51**, 1087–1102 (2003)
31. P. Hurley, P. Bate, F. Humphreys, An objective study of substructural boundary alignment in aluminium. Acta Mater. **51**, 4737–4750 (2003)
32. F. Humphreys, P. Prangnell, J.R. Bowen, A. Gholinia, C. Har- ris, Developing stable fine–grain microstructures by large strain deformation, . Philos. Trans. R. Soc. Lond. Ser. A Math. Phys. Eng. Sci. **357**, 1663–1681 (1999)
33. I. Beyerlein, R. Lebensohn, C. Tome, Modeling texture and microstructural evolution in the equal channel angular extrusion process. Mater. Sci. Eng. A. **345**, 122–138 (2003)
34. W. Abdel-Aziem, A. Hamada, T. Makino, M. Hassan, Microstructural evolution during extrusion of equal channel angular-pressed AA1070 alloy in micro/mesoscale, Materials Science and Technology 1–9 (2020).
35. J.N. Florando, B.S. El-Dasher, C. Chen, D.C. Swift, N.R. Barton, J.M. McNaney, K.T. Ramesh, K.J. Hemker, M. Kumar, Effect of strain rate and dislocation density on the twinning behavior in tantalum. AIP Adv. **6**, 045120 (2016)
36. J. Lee, H. Jeong, Effect of rolling speed on microstructural and microtextural evolution of Nb tubes during caliber-rolling process. Metals. **9**, 500 (2019)
37. P. Klimanek, A. Pötzsch, Microstructure evolution under compressive plastic deformation of magnesium at different temperatures and strain rates. Mater. Sci. Eng. A. **324**, 145–150 (2002)
38. Y. Li, Y. Zhang, N. Tao, K. Lu, Effect of the Zener-Hollomon parameter on the microstructures and mechanical properties of Cu subjected to plastic deformation. Acta Mater. **57**, 761–772 (2009)
39. A. Sarkar, J. Chakravartty, Activation volume and density of mobile dislocations in plastically deforming Zr-1pctSn- 1pctNb-0.1 pctFe alloy. Metall. Mater. Trans. A. **46**, 5638–5643 (2015)
40. K. Hoge, A. Mukherjee, The temperature and strain rate dependence of the flow stress of tantalum. J. Mater. Sci. **12**, 1666–1672 (1977)
41. S. Lau, S. Ranji, A. Mukherjee, G. Thomas, J. Dorn, Dislocation mechanisms in single crystals of tantalum and molybdenum at low temperatures. Acta Metall. **15**, 237–244 (1967)
42. J. Wang, Q. Duan, C. Huang, S. Wu, Z. Zhang, Tensile and compressive deformation behaviors of commercially pure Al processed by equal-channel angular pressing with different dies. Mater. Sci. Eng. A. **496**, 409–416 (2008)
43. M. Lipińska, L. Olejnik, A. Pietras, A. Rosochowski, P. Bazarnik, J. Goliński, T. Brynk, M. Lewandowska, Microstructure and mechanical properties of friction stir welded joints made from ultrafine grained aluminium 1050. Mater. Des. **88**, 22–31 (2015)
44. P. Verleysen, W. Oelbrandt, S. Naghdy, L. Kestens, Static and dynamic tensile behaviour of aluminium processed by high pressure torsion, EPJ Web of Conferences, EDP Sciences, 2015, pp. 02012.

45. N. Hansen, Hall-Petch relation and boundary strengthening. Scripta Mater. **51**, 801–806 (2004)
46. P. Kusakin, A. Belyakov, D.A. Molodov, R. Kaibyshev, On the effect of chemical composition on yield strength of TWIP steels. Mater. Sci. Eng. A. **687**, 82–84 (2017)
47. T. Koizumi, M. Kuroda, Grain size effects in aluminum processed by severe plastic deformation. Mater. Sci. Eng. A. **710**, 300–308 (2018)